

A systematic study of Zr and Sn isotopes in the Relativistic Mean Field theory

L. S. Geng

*Research Center for Nuclear Physics (RCNP), Osaka University,
Ibaraki, Osaka 567-0047, Japan
School of Physics, Peking University, Beijing 100871, P.R. China
lsgeng0@rcnp.osaka-u.ac.jp*

H. Toki

*Research Center for Nuclear Physics (RCNP), Osaka University,
Ibaraki, Osaka 567-0047, Japan
toki@rcnp.osaka-u.ac.jp*

J. Meng

*School of Physics, Peking University, Beijing 100871, P.R. China
mengj@pku.edu.cn*

The ground-state properties of Zr and Sn isotopes are studied within the relativistic mean field theory. Zr and Sn isotopes have received tremendous attention due to various reasons, including the predicted giant halos in the neutron-rich Zr isotopes, the unique feature of being robustly spherical in the region of $^{100}\text{Sn} \sim ^{132}\text{Sn}$ and the particular interest of Sn isotopes to nuclear astrophysics. Furthermore, four (semi-) magic neutron numbers, 40, 50, 82 and 126, make these two isotopic chains particularly important to test the pairing correlations and the deformations in a microscopic model. In the present work, we carry out a systematic study of Zr and Sn isotopes from the proton drip line to the neutron drip line with deformation effects, pairing correlations and blocking effects for nuclei with odd number of neutrons properly treated. A constrained calculation with quadrupole deformations is performed to find the absolute minimum for each nucleus on the deformation surface. All ground-state properties, including the separation energies, the odd-even staggerings, the nuclear radii, the deformations and the single-particle spectra are analyzed and discussed in detail.

1. Introduction

One of the main aims of researches in nuclear physics is to describe the ground-state properties of all nuclei in the periodic table with one method. Unfortunately, due to lack of understanding in strong interaction and numerical difficulties in handling nuclear many-body problems, so far all microscopic descriptions are only possible on a phenomenological ground. The most successful theories of this type are the conventional Hartree-Fock method with effective density-dependent interactions^{1,2,3} and its relativistic analog, the relativistic mean field (RMF) theory^{4,5,6}. The Hartree-Fock method is based on the non-relativistic kinematics, in which the spin-orbit

interaction and the density dependent interaction are important ingredients. While the RMF theory is based on the relativistic kinematics, in which the nucleons, the mesons and their interactions are the ingredients. Therefore, the spin appears automatically and the interplay of the scalar and the vector potentials leads naturally to a proper spin-orbit interaction and appropriate shell structure. Such a property is very important for the extrapolation of a phenomenological model to study exotic nuclei, which have become accessible in recent years due to developments in accelerator technology and detection techniques⁷. The RMF theory has been very successful for the description of many nuclear properties including binding energies, nuclear radii and deformations from the proton drip line to the neutron drip line^{8,9}. However, the number of nuclear properties investigated by the RMF model is still considerably less than those done by its non-relativistic counterpart.

To describe nuclear ground-state properties over a wide mass region properly, we must take into account both deformation effects and pairing correlations simultaneously. It has been known for a long time that most nuclei except for a few with and near magic numbers are deformed and most of them can be described by axial deformations. In the present work, we adopt the expansion method in the Harmonic-Oscillator basis to describe the single-particle wave functions in the deformed mean field potential¹⁰. In the original work of Gambhir. et al.¹⁰, the pairing correlations are treated in the BCS framework using a constant pairing interaction with a pairing window. This method has been found to be incapable of describing exotic nuclei where the continuum effects become important near the drip lines. On the other hand, recently it was demonstrated that the use of a zero-range δ -force in the particle-particle channel was able to take into account the couplings to the continuum nicely in the non-relativistic mean field models^{11,12}. This BCS framework with the zero-range δ -force has been introduced into the relativistic mean field models with the spherical shape^{13,14,15,16,17}. The zero-range δ -force acting on the paired nucleons in the BCS framework is able to pick up the states (resonant states) having a large overlap with the occupied states below the Fermi surface^{11,15,16,17}. We, therefore, have introduced the zero-range δ -force in the BCS framework into the expansion method¹⁰ in the deformed RMF model and demonstrated its applicability in Ref.¹⁸. This method has been applied to study the properties of light nuclei¹⁹, particularly the proton-skins in the Ar isotopic chain and the neutron-skins in the Na isotopic chain, and the alpha-decay properties of the lately synthesized superheavy elements 115 and 113²⁰. When applying this method to the neutron-rich nuclei, due to their large spacial extension, we do not expect the description of the sudden increase of neutron radii in halo nuclei, which were found if we had solved the RMF equations in coordinate space^{16,18,21}. However, except for the neutron radii of the halo nuclei, other properties could be reproduced with satisfactory accuracy by this method¹⁸. One way out of this deficiency for the description of halo nuclei is to use the expansion method in the Woods-Saxon basis²⁸, which unfortunately is only possible for spherical nuclei at present.

The Zr and Sn isotopic chains have received lots of attention for a long time.

The Zr isotope has a semi-magic proton number 40, and its neutron number can be (semi-) magic numbers 40, 50 and 82. Most recently, several RMF calculations show that the so-called giant halos may occur in the Zr isotopic chain where neutron number goes beyond 82^{16,18,21}. The evolution of deformation, the potential energy surfaces, the microscopic structure of coexisting configurations, and shape transitions in heavy Zr isotopes have been discussed extensively since a long time ago (see Refs. ^{22,23,24}), where sophisticated models have been employed and detailed analyses have been made. In the present work, our discussions of the evolution of the deformation in the Zr isotopic chain (including that of the Sn isotopic chain) are restricted to the mean field level. We would like to also compare our predictions with those of two of the most successful non-relativistic mean field models, the finite-range droplet model (FRDM)²⁵ and the Hartree Fock + BCS method (HF+BCS)²⁶. We notice that the effect of the proton-neutron pairing for ⁸⁰Zr is also revisited lately²⁷.

The Sn isotope has long been of special interest for nuclear physicists not only because it has a magic proton number 50, but also due to its extremely long isotopic chain. Experimentally both the double magic nuclei, the neutron-deficient ¹⁰⁰Sn and the neutron-rich ¹³²Sn, have been produced. We expect that its isotopes will even extend to the next neutron magic number, $N = 126$, which will be one of the objects of the present study. Most Sn isotopes have been found to be spherical both experimentally and theoretically, particularly those nuclei with $N = 50 \sim 82$, but whether or not such a trend can continue to the next neutron-magic number, $N = 126$, remains to be an interesting and yet open question. Recently, Samanta et al. suggested that the Pb isotope ($Z = 82$) loses its magicity around $N = 106$ based on the extended Bethe-Weizsäcker mass formula²⁹. This motivates us to study also the magicity of $Z = 50$ by the RMF method. The RMF model is particularly suitable for such a purpose because of its natural description of spin-orbit interaction. Just like Zr isotopes, Sn isotopes have also been investigated quite a lot both in relativistic^{30,31,32} and non-relativistic mean field³³ models. However, most of them are limited to either spherical assumptions, or even-even nuclei, or just part of the isotopic chain. The same limitations are also true for Zr isotopes.

In the present work, we apply the recently formulated deformed RMF+BCS method with a zero-range δ -force in the pairing channel^{18,19,20} to the analysis of the ground-state properties of Zr and Sn isotopes from the proton drip line to the neutron drip line. In particular, we would like to study the neutron-rich nuclei in both isotopic chains and the magicity of $Z = 50$ in the neutron-rich region. We use the TMA³⁴ and NL3³⁵ parameter sets for the RMF Lagrangian density, which are two of the most successful parameter sets in the relativistic mean field model. In Sec. 2, we briefly present the RMF model with deformation effects and pairing correlations. The numerical details and discussions will be presented in Sec. 3 and a summary of the present study is given in Sec. 4.

4 *L. S. Geng, H. Toki, and J. Meng*

2. Relativistic mean field model with deformation effects and pairing correlations

We briefly present here the formulation of the RMF model with deformation effects and pairing correlations. We employ the model Lagrangian density with nonlinear terms for both σ and ω mesons, as described in detail in Ref. 18,34, which is given by

$$\begin{aligned} \mathcal{L} = & \bar{\psi}(i\gamma^\mu\partial_\mu - M)\psi + \frac{1}{2}\partial_\mu\sigma\partial^\mu\sigma - \frac{1}{2}m_\sigma^2\sigma^2 - \frac{1}{3}g_2\sigma^3 - \frac{1}{4}g_3\sigma^4 - g_\sigma\bar{\psi}\sigma\psi \\ & - \frac{1}{4}\Omega_{\mu\nu}\Omega^{\mu\nu} + \frac{1}{2}m_\omega^2\omega_\mu\omega^\mu + \frac{1}{4}g_4(\omega_\mu\omega^\mu)^2 - g_\omega\bar{\psi}\gamma^\mu\psi\omega_\mu \\ & - \frac{1}{4}R^a{}_{\mu\nu}R^{a\mu\nu} + \frac{1}{2}m_\rho^2\rho_\mu^a\rho^{a\mu} - g_\rho\bar{\psi}\gamma^\mu\tau^a\psi\rho_\mu^a \\ & - \frac{1}{4}F_{\mu\nu}F^{\mu\nu} - e\bar{\psi}\gamma_\mu\frac{1-\tau_3}{2}A^\mu\psi, \end{aligned} \quad (1)$$

where the field tensors of the vector mesons and of the electromagnetic field take the following forms:

$$\begin{cases} \Omega_{\mu\nu} = \partial_\mu\omega_\nu - \partial_\nu\omega_\mu \\ R^a{}_{\mu\nu} = \partial_\mu\rho_\nu^a - \partial_\nu\rho_\mu^a - 2g_\rho\epsilon^{abc}\rho_\mu^b\rho_\nu^c \\ F_{\mu\nu} = \partial_\mu A_\nu - \partial_\nu A_\mu \end{cases} \quad (2)$$

and other symbols have their usual meanings. Based on the single-particle spectra calculated by the RMF method, we perform a state-dependent BCS calculation 18,36,37. The gap equation has a standard form for all the single particle states. i.e.

$$\Delta_k = -\frac{1}{2} \sum_{k'>0} \frac{\bar{V}_{kk'}\Delta_{k'}}{\sqrt{(\varepsilon_{k'} - \lambda)^2 + \Delta_{k'}^2}}, \quad (3)$$

where $\varepsilon_{k'}$ is the single particle energy and λ is the Fermi energy. The particle number condition is given by $2 \sum_{k>0} v_k^2 = N$. As have been done in the recent works 18,19,20, a zero-range δ -force $V = -V_0\delta(\mathbf{r}_1 - \mathbf{r}_2)$ is used in the particle-particle channel in order to take into account the continuum effects properly. For nuclei with odd number of nucleons, a simple blocking method without breaking the time-reversal symmetry is adopted. The ground state of an odd system is described by the wave function,

$$\alpha_{k_1}^\dagger|BCS\rangle = \alpha_{k_1}^\dagger \prod_{k \neq k_1} (u_k + v_k\alpha_k^\dagger\alpha_k^\dagger)|vac\rangle. \quad (4)$$

Here, $|vac\rangle$ denotes the vacuum state. The unpaired particle sits in the level k_1 and blocks this level. The Pauli principle prevents this level from participating in the scattering process of nucleons caused by the pairing correlations. As described in Ref. 19,37, the gap equation with one level k_1 ‘‘blocked’’ has the form:

$$\Delta_k = -\frac{1}{2} \sum_{k' \neq k_1 > 0} \frac{\bar{V}_{kk'}\Delta_{k'}}{\sqrt{(\varepsilon_{k'} - \lambda)^2 + \Delta_{k'}^2}}, \quad (5)$$

with the corresponding chemical potential determined by $N = 1 + 2 \sum_{k \neq k_1 > 0} v_k^2$. This blocking procedure is performed at each step of the self-consistent iteration and more numerical details will be discussed below.

3. Numerical details and discussions

3.1. *The convergence study*

For heavy nuclei more Harmonic-Oscillator shells in the expansion of fermion and boson fields have to be used in order to achieve reliable convergence. However, computation time increases dramatically with the increase of the number of shells. The common procedure to tackle this problem is to limit the number of shells by studying the convergence behavior in the region of interest. For this reason, we investigate in detail three nuclei ^{132}Sn , ^{176}Sn and ^{130}Zr , which are chosen to represent spherical neutron-rich nuclei, spherical drip-line nuclei and deformed halo nuclei. For the case of ^{132}Sn , with the basis parameter $\beta_0 = 0.0$, it is found that for $N = N_f = N_b \geq 14$, where N_f and N_b are the numbers of shells used in the expansion of fermion and boson fields, the desirable convergence is obtained properly. The increase of N from 14 to 20 changes the total binding energy B and the binding energy per particle B/A by about 0.2%, while the rms charge radii R_c is changed by 0.1% and the rms neutron radii R_n is changed by 0.3%. For ^{132}Sn , even 12 shells can obtain the satisfactory convergence as shown in Table I. Similar conclusion can be made for ^{176}Sn (Table II) except that now a minimum of 14 shells is needed. Things are a little bit different for ^{130}Zr (Table III), which has been predicted to be a halo nucleus²¹. With N increasing from 14 to 20, B and B/A change by about 0.6%, while R_c is changed by 0.1%, and R_n is changed by 0.7%. In our calculations the ground state of ^{130}Zr has a deformation of $\beta_{2m} = -0.203$. Setting β_0 equal to -0.209 , we find that β_{2m} is changed by about 3% when N increases from 14 to 20.

In conclusion, we find that 14 shells are enough for a correct description of B , B/A , R_c and β_2 . While for R_n , to describe the halo nuclei more reliably, shells more than 14 are needed. Of course, as is well known (see Ref. ²⁸ and references therein), the rms neutron radii of neutron halo nuclei can not be fully reproduced within the Harmonic-Oscillator basis even with a large number of basis. Keeping all these in mind, we decide to use 20 shells ($N_f = N_b = 20$) for the calculations with the TMA parameter set, while for the calculations with the NL3 parameter set 14 shells ($N_f = N_b = 14$) are used to save computation time.

3.2. *The blocking method and the pairing strength*

As we have stated in Sec. 2, for nuclei with odd number of neutrons a blocking method without breaking the time-reversal symmetry is adopted in the self-consistent calculation. At each step, the state to be blocked is determined by counting the single-particle spectra from the bottom. Then with this state blocked, the

6 *L. S. Geng, H. Toki, and J. Meng*

BCS calculation is performed. This procedure is repeated until the required convergence is obtained. The same procedure is also adopted in the constrained calculations. For each nucleus, first the constrained calculation³⁸ is done to obtain all possible ground-state configurations; second we perform the non-constrained calculation using the quadrupole deformation parameter of the deepest minimum of the energy curve of each nucleus as the deformation parameter for the Harmonic-Oscillator basis. In the case of several similar minima from the constrained calculation, the non-constrained calculation is repeated around each minimum to obtain the configuration with the lowest energy as the final result.

We note that the most appropriate way to perform blocking calculations is by blocking all orbits accessible to the odd nuclei at each deformation, but it is incredibly time consuming. Therefore, our method should be seen as an approximation to that kind of full calculation and the agreement should be checked at certain points. Here we take ^{151}Sn in our RMF+BCS calculations with the TMA parameter set as an example to show the validity of this method. First, the constrained calculation finds that the deepest minimum is at $\beta_2 \approx -0.263$. Using this as the basis deformation, i.e. $\beta_0 = -0.263$, we perform the non-constrained calculation. The final result is $B = 1142.791$ with $\beta_2 = -0.266$, where B is the total binding energy. Looking at the single-particle spectra, we find that the blocked state is $1/2^- [521]$ with the single-particle energy $E = -2.239$. Two other possible states accessible to the odd neutron is $3/2^- [521]$ with $E = -2.374$ and $11/2^+ [615]$ with $E = -2.156$. If one of these two states were blocked instead of $1/2^- [521]$, the results would be $B = 1142.728$ with $\beta_2 = -0.267$ and $B = 1142.659$ with $\beta_2 = -0.267$. These are all close to each other and our method chooses the correct configuration with the lowest energy. This case shows that the procedure we adopted works very well. However, there are cases where the state chosen by this procedure does not lead to the “absolute minimum”. Nevertheless, such wrong selections of the blocking states generally lead to a difference less than 0.2 MeV for the total binding energy, which is actually beyond the accuracy of our calculations and therefore can be safely ignored.

The pairing strength $V_0 = 341.1 \text{ MeV fm}^3$ is used for Zr isotopes and $V_0 = 310.0 \text{ MeV fm}^3$ for Sn isotopes, which are obtained by fitting the experimental odd-even staggering (OESs) of Zr and Sn isotopes with a cut-off $E_{max} - \lambda \leq 8.0 \text{ MeV}$. We use the same pairing strength for both protons and neutrons. For comparison, calculations have been done with the NL3 parameter set also, but only for even-even nuclei. The pairing strength is kept the same for calculations with both the TMA parameter set and the NL3 parameter set.

3.3. Neutron separation energies and binding energies

The double and single neutron separation energies

$$S_{2n}(Z, N) = B(Z, N) - B(Z, N - 2), \quad (6)$$

$$S_n(Z, N) = B(Z, N) - B(Z, N - 1), \quad (7)$$

are displayed in Figs. 1 and 2 for Zr isotopes and Sn isotopes, respectively, from the proton drip line to the neutron drip line. The results obtained from the deformed RMF+BCS calculations with the parameter set TMA are compared with available experimental data³⁹. In the upper panels of Figs. 1 and 2, the results obtained from the deformed RMF+BCS calculations with the NL3 parameter set are also shown for comparison. It is clearly seen that both experimental separation energies and OESs are reproduced quite well by the theoretical calculations. The RMF+BCS calculations with different parameter sets TMA and NL3 also agree with each other very well.

For Zr isotopes, despite of the fact that the variation of the deformation is quite complicated for the whole isotopic chain (see Figs. 4 and 6), the agreement between theory and experiment is very good. The experimental feature that the OESs are larger for nuclei with $N = 40 \sim 50$ than for nuclei with $N = 51 \sim 68$ is also reproduced quite well. Both the double and single neutron separation energies are quite small for nuclei with $N > 82$. The so-called giant halos are predicted to exist in this region by both the RCHB²¹ and the resonant RMF+BCS¹⁶ calculations with spherical assumptions. Our previous deformed RMF+BCS calculations¹⁸ reached the same conclusion and confirmed that the expansion method in the Harmonic-Oscillator basis can provide very accurate results for nuclear binding energies even in the neutron-rich region. All these calculations^{16,18,21}, however, are limited to only even-even nuclei. From the lower panel of Fig. 1, we notice that the OESs of Zr isotopes with $N > 82$ are quite small and S_n of those nuclei with odd mass numbers are almost zero or negative. This is easy to understand because the pairing correlations can increase the binding energies of even-even nuclei more and therefore contribute to the formation of halo nuclei. We also conclude that generally we will see one-neutron halo nucleus first and then only two-neutron halo nucleus is stable due to the pairing correlations. The same conclusion also holds for Sn isotopes.

For Sn isotopes, we notice that the agreement between theory and experiment is very good in the region, $^{115}\text{Sn} \sim ^{132}\text{Sn}$. The two-neutron drip-line nucleus is predicted to be ^{176}Sn by our calculations with both the TMA and the NL3 parameter sets, which agree well with the calculations with other parameter sets in the RMF framework⁴⁰. This seems to be a unique feature of the RMF calculations while the HF calculations usually shift the drip-line nucleus toward the light mass region (see Fig. 4 of Ref. ⁴¹). Different isospin dependence and spin-orbit description could be the reason why this discrepancy happens. However, since we are talking about exotic nuclei far from the stability region, this remains to be an open question anyway. For nuclei with $N \leq 64$, the theoretical OES drops a little bit suddenly. The reason behind this is a relatively large spin-orbit splitting between $2d_{5/2}$ state and $2d_{3/2}$ state, around 1.8 MeV in our present calculations (see Figs. 7 and 8), which makes pairing energy in nuclei with $N \leq 64$ smaller than in nuclei with $N = 64 \sim 82$. We note that the smaller OES in the region of $^{146}\text{Sn} \sim ^{160}\text{Sn}$ is quite complicated and may be related with two different phenomena. One is that nuclei in this region are deformed (see Fig. 5). The other one is that as we shall see from Fig. 8, the $3p_{1/2}$,

8 *L. S. Geng, H. Toki, and J. Meng*

$2f_{5/2}$ and $3p_{3/2}$ states, which become occupied in this region, are quite close to each other. In both Zr and Sn isotopic chains, we should note that for nuclei with $N \approx Z$ additional residual interactions, such as the proton-neutron pairing, will contribute and increase the OES somewhat, which are not included in the present model. Unlike Zr isotopes, we do not see a clear indication of possible two-neutron halo in the Sn isotopic chain, which is consistent with all previous calculations. The double neutron separation energy goes directly to about -2.5 MeV for ^{178}Sn from about 1.4 MeV for ^{176}Sn . However, from the lower panel of Fig.2, we can see that S_n stays below 1.0 MeV from ^{157}Sn till the end of this isotopic chain, which implies the possible existence of one-neutron halo.

The average binding energy per particle is plotted as a function of mass number A in Fig. 3 for Zr and Sn isotopes. It can be clearly seen that the theoretical predictions reproduce the experimental data accurately including the OESs in Sn isotopes. For Zr isotopes, the small deviation between theory and experiment for nuclei with $N = 52 \sim 58$ is probably related with the particle number non-conservation feature of the present BCS method, which will be discussed more below. For Sn isotopes around $N \approx Z$, our calculated results are somewhat larger than the experimental data.

3.4. Deformation properties

Deformation is quite an important property for nuclei. It can increase the nuclear binding energy so that a deformed shape is more favored than the spherical shape for certain nuclei. The deformation effect is also important for the description of odd-even staggering (OES). It has been argued that in light- or medium-mass nuclei deformation provides the same amount of OES as the pairing interaction⁴² and/or that the OES in light nuclei is a mere reflection of the deformed mean field⁴³. Although it is believed that the OES in heavy nuclei is mainly due to the pairing correlations, the deformation effect should never be ignored. We have also shown in Ref.¹⁸ that the deformation effect in even-even Zr isotopes is quite important to reduce the discrepancy between the theoretical and the experimental binding energies. $Z = 50$ has long been seen as a special magic number in the sense that all Sn isotopes are believed to be spherical. Whether or not Sn isotopes are deformed also is of special interest to the synthesis of nuclei in the astrophysical r-process.

In Figs. 4 and 5, we plot the mass quadrupole deformation parameters, β_2 , for Zr and Sn isotopes. The results of our calculations with the TMA and NL3 parameter sets are compared with those of the finite-range droplet model (FRDM)²⁵ and the Hattie Fock + BCS (HF+BCS)²⁶ method. The experimental data are extracted from the $B(E2)$ values given in Ref.⁴⁴.

From Fig. 4, it is seen that the variation of the deformation is quite complicated for Zr isotopes. The agreement between different theoretical calculations, RMF+BCS/TMA, RMF+BCS/NL3, FRDM and HF+BCS, and experimental data is quite good in general. Nuclei with $N \leq 80$ are very deformed in all the theoretical

calculations. The same is true for nuclei with $58 \leq N \leq 70$. Nuclei with $N > 88$ are moderately deformed with $\beta_2 \approx 0.3$ by FRDM and $\beta_2 \approx -0.3$ by RMF+BCS with both the TMA and NL3 parameter sets, while HF+BCS seems to prefer spherical shapes for this region. There are two regions where the theoretical calculations do not agree so well with each other. The first one is around $42 \leq N \leq 54$, where the results of FRDM and RMF+BCS/NL3 stay almost spherical while HF+BCS and RMF+BCS/TMA show signs of oscillation between oblate and prolate shapes. The second region is about $70 < N < 80$, where both RMF+BCS/TMA and FRDM predict oblate shapes while RMF+BCS/NL3 and HF+BCS prefer spherical configurations. These discrepancies between different theoretical calculations indicate that the nuclei in these regions are “soft” in the sense of deformation (see also Fig. 6).

However, Sn isotopes are quite different from Zr isotopes. It remains robustly spherical till N reaches 88 in all the theoretical calculations. Then the non-relativistic calculations FRDM and HF+BCS show a region of moderately deformed with $\beta_2 \approx 0.3$ around $90 < N < 110$. The relativistic calculations show a transition from prolate shapes ($90 < N < 100$) to oblate shapes ($100 < N < 110$) while the amplitudes of deformation are similar to their non-relativistic counterparts. For nuclei with N approaching the magic number 126, the RMF+BCS calculations and the HF+BCS calculations predict spherical shapes while the FRDM calculations prefer prolate configurations. It is quite a surprise that all the theoretical works, either non-relativistic or relativistic, predict a deformed region around $90 < N < 110$ for Sn isotopes, which makes our predictions well grounded. Although it may be trivial, another well-known feature shown in our calculations is that the even-odd nucleus tends to be deformed despite that its neighboring even-even nuclei are spherical. Of course at most times, the deformation is quite small and we can say that it is essentially spherical. Most even-odd Sn isotopes with $N < 82$ belong to this group. However, in Zr isotopes, some even-odd nuclei differ from their even-even neighbors by an absolute β_2 of 0.1. ^{87}Zr , ^{89}Zr , ^{117}Zr and ^{119}Zr are such nuclei.

Usually, we can find two minima on the total energy surface of an axially deformed nucleus, one prolate and the other oblate, or spherical. On the theoretical side, it is easy to tell which one is the ground-state configuration if the difference between the total energies of different minima is relatively large. On the other hand, nuclei in transition region often have two minima with similar total energies, where it is difficult to determine the ground state without ambiguity. ^{82}Zr , ^{86}Zr , ^{93}Zr and ^{116}Zr are such nuclei in the Zr isotopic chain. We display their total energy curves together with those of 12 other Zr isotopes as functions of β_2 in Fig. 6. It provides us a vivid picture how deformation evolves in Zr isotopes. Nuclei with $A < 82$ are strongly prolate with $\beta_2 \approx 0.5$. At ^{82}Zr , the oblate configuration becomes as stable as the prolate configuration. Nuclei with $82 < A < 86$ are moderately oblate with $\beta_2 \approx -0.2$. At ^{86}Zr , the total energy curve becomes quite flat at the bottom and the spherical configuration is a little bit more stable. With increasing N , even-even nuclei stay almost spherical while even-odd nuclei are somewhat deformed. At ^{93}Zr ,

the prolate configuration $\beta_2 \approx 0.2$ is more stable than the oblate configuration $\beta_2 \approx -0.1$. Nuclei with increasing N become more prolate and β_2 reaches 0.4 at ^{109}Zr . Then ^{110}Zr becomes oblate and β_2 begins to approach zero with increasing N . At ^{116}Zr , the spherical configuration is reached and maintained for even-even nuclei till ^{124}Zr . Then the nucleus with more neutrons become more prolate till ^{129}Zr and from ^{130}Zr it stays moderately oblate, $\beta_2 \approx -0.2$, till the end of this isotopic chain. It will be very interesting to study shape-coexistences in the whole Zr isotopic chain within the relativistic mean field model just as what have been done in the non-relativistic models (see Refs. ^{23,24}) and compare with experimental data, if available. (Here it should be noted that the different minima on the potential energy surfaces may be linked by a valley in the gamma angle, so that a secondary minimum might imply a gamma-soft structure or even indicate a triaxial structure, which of course is not supposed to be seen in the present work due to the assumption of axial symmetry.)

We would like to make a few more comments about the discrepancy between theory and experiment in the region of $N = 52 \sim 58$ in the Zr isotopic chain. Experimentally ⁴⁴, the nuclei ^{92}Zr , ^{94}Zr , ^{96}Zr and ^{98}Zr are almost spherical and nuclei with $N \geq 60$ suddenly become very deformed. While in our calculations (including those of FRDM and HF+BCS models), the nucleus becomes deformed gradually from $N = 52$ with N and agrees with experiment after $N = 60$. The reason could be that the current BCS method mixes the wave functions with different particle number and therefore leads to finite deformation for the nuclei in the region of $N = 52 \sim 58$. A calculation with an improved BCS method that conserves the particle number could clarify this discrepancy and this work is in progress now.

3.5. *Single-particle spectra of Sn isotopes*

It has long been known that the nuclear deformation is caused by the interplay between protons and neutrons (see Ref. ²³ and references therein). In this sense, the reliability of the deformation developments predicted by our calculations are more or less determined by to what extent the relativistic mean field theory with the particular parameter sets TMA and NL3 can reproduce the experimental single-particle spectra, particularly the proton gap at $Z = 50$ and the neutron gap at $N = 82$. In Fig. 7, the single-particle energies of ^{132}Sn calculated with the parameter sets TMA and NL3 are compared with the experimental single-particle energies ^{40,45} for protons (left panel) and neutrons (right panel). It is very clear that the calculations with both the TMA parameter set and the NL3 parameter set agree with each other very well and are also in reasonable agreement with the experimental single-particle spectra. The proton gap at $Z = 50$ is reproduced quite well by NL3, while TMA predicts a gap of 0.5 MeV smaller than experiment. Meanwhile, the calculated neutron gap at $N = 82$ is somewhat larger than experiment for both parameter sets. We should note that such a comparison is not very well defined and a detailed analysis of the single-particle spectra in the relativistic mean field theory

can be found in Ref. ⁴⁵. Anyway, the good agreement with the experimental data justifies us to extend the relativistic mean field model to the study of exotic nuclei.

In our above discussions, some small discrepancies in the single-neutron separation energies for Sn isotopes with $N < 64$ have been attributed to their single-particle spectra. The abnormalities in the region of $^{146}\text{Sn} \sim ^{160}\text{Sn}$ are also related to the corresponding shell structures. To see all these more clearly, we display the neutron single-particle spectra of five nuclei in Sn isotopes, i.e. ^{100}Sn , ^{114}Sn , ^{132}Sn , ^{158}Sn and ^{176}Sn in Fig. 8. These isotopes are so chosen to represent the whole Sn isotopes from the proton drip line to the neutron drip line and also include two typical nuclei in the region where the predicted OES changes abruptly. All the five nuclei are spherical in our calculations. It is quite clear that the $1h_{11/2}$, $3s_{1/2}$ and $2d_{3/2}$ states are quite close to each other, which explains the somewhat large difference in the OES between nuclei with $N > 64$ and $N < 64$, together with the relatively large gap between the $2d_{3/2}$ state and the $2d_{5/2}$ state. The small gap between the $3p_{1/2}$, $2f_{5/2}$ and $3p_{3/2}$ states is possibly responsible for both the deformation phenomena and abnormalities in the OES in the region of $^{146}\text{Sn} \sim ^{160}\text{Sn}$.

There are also some other important features shown in Fig. 8. First, the neutron level density increases with N : the single-particle energy of the $1s_{1/2}$ state increases about 10.0 MeV from -62.0 MeV in ^{100}Sn to -52.0 MeV in ^{176}Sn ; meanwhile, the single-particle energy of the $1g_{9/2}$ state decreases about 2.0 MeV. Second, it is quite clear that the spin-orbit splitting also decreases with increasing N . Some obvious spin-orbit partners, which exhibit this feature well, are $(1p_{1/2}, 1p_{3/2})$, $(1d_{3/2}, 1d_{5/2})$, $(1f_{5/2}, 1f_{7/2})$ and $(1g_{7/2}, 1g_{9/2})$. The decrease of spin-orbit splitting with increasing N in the relativistic mean field theory has been discussed in several previous works (see Ref. ³¹), where it has been attributed to the diffuseness of the potential.

3.6. Nuclear radii and neutron skin

From the proton (neutron) density distributions, $\rho_{p(n)}$, we can easily deduce the corresponding proton (neutron) radius,

$$R_{p(n)} = \langle r_{p(n)}^2 \rangle^{1/2} = \left[\frac{\int \rho_{p(n)} r^2 d\mathbf{r}}{\int \rho_{p(n)} d\mathbf{r}} \right]^{1/2}. \quad (8)$$

The charge radius, R_c , is related to the proton radius, R_p , after considering the finite size of the proton, by

$$R_c^2 = R_p^2 + 0.64 \quad [\text{fm}]. \quad (9)$$

We display in Figs. 9 and 10 the charge, proton and neutron rms radii for Zr and Sn isotopes. The calculated charge radii are compared with the experimental data from Ref. ⁴⁶. Excellent agreement between theory and experiment can be clearly seen. We can also see the effect of deformation clearly from Figs. 9 and 10. In the upper panel of Fig. 9, R_c of Zr isotopes drops dramatically for ^{82}Zr and ^{110}Zr , which is due to the deformation effect. If we take a look at Fig. 4, it becomes much clearer:

β_{2p} changes from 0.535 for ^{81}Zr to -0.218 for ^{82}Zr ; correspondingly, β_{2p} changes from 0.418 for ^{109}Zr to -0.216 for ^{110}Zr . There are also some abnormalities in Sn isotopes as we can see in the upper panel of Fig. 10, which have the same origins as Zr isotopes. β_{2p} jumps from 0.085 for ^{144}Sn to 0.220 for ^{145}Sn and it changes from -0.244 for ^{157}Sn to 0.0 for ^{158}Sn .

In the lower panels of Figs. 9 and 10, we plot R_n and R_p together in order to see the differences between them easily. We also display a solid line with a $N^{1/3}$ dependence in both panels for R_n . It is quite clear that the neutron-rich nuclei in Zr isotopes deviate from the $N^{1/3}$ line quite a lot, which implies that the giant halos exist even though deformation develops after $N = 82$. While for Sn isotopes our calculated results agree well with the $N^{1/3}$ line. The difference between R_n and R_p , i.e. neutron skin, reaches 0.9 fm for ^{140}Zr and 0.8 fm for ^{176}Sn , which can be viewed as another indication of possible neutron halo in Zr isotopes. Of course, we should note that as we have found in our previous work¹⁸, the sudden increase of the neutron radii in $^{124}\text{Zr} \sim ^{140}\text{Zr}$, predicted by the RCHB²¹ and the resonant RMF+BCS¹⁶ calculations, can not be fully reproduced by the expansion method in the Harmonic-Oscillator basis. Nevertheless, this should not prevent us from gaining some useful insights into possible neutron halo feature, as we can see in Zr isotopes where a sudden increase in neutron radii from ^{123}Zr is quite obvious.

4. Conclusions

It is our strong desire to develop a model valid for all nuclei, including unstable ones from the proton drip line to the neutron drip line. The relativistic mean field theory, as a relativistic method which incorporates spin-orbit interaction naturally, hopefully can be the desirable model with only a few parameters fitted by the saturation properties of nuclear matter and the ground-state properties of a few well-known spherical nuclei. However, to describe nuclei over a wide mass region, deformation effects and pairing correlations must be taken into account simultaneously and in a proper way. The present method we adopted can fulfill all these requirements nicely and cost reasonable time to carry out large-scale calculations covering all nuclei from the proton drip line to the neutron drip line, which are necessary to test a phenomenological method and provide reliable information for both experimental physicists and other related subjects.

In the present work, we have studied two of the most interesting isotopic chains in the periodic table, Zr and Sn, from the proton drip line to the neutron drip line. This is the first of such kind of calculations carried out in the relativistic mean field model for the whole Zr and Sn isotopic chains including deformation effects and proper pairing correlations. Our calculations reproduce the available experimental data very well including the nuclear binding energies, the separation energies, the odd-even staggering (OESs), and the nuclear radii. In particular, nuclear deformations are analyzed in detail for both Zr and Sn isotopes in the mean field level. Remarkable agreements with the very successful non-relativistic

theoretical models, the FRDM model and the HF+BCS method, are observed. Surprisingly, we find that Sn isotopes are deformed in the region of $N = 89 \sim 107$. The fact that all theoretical works reach the same conclusion makes our predictions well grounded. ^{176}Sn is found to be the last stable nucleus against neutron emission in the Sn isotopic chain and the predicted halo phenomena in the Zr isotopic chain are confirmed once again.

Here, it is necessary to mention the mass dependence of the parameter set TMA. There are several reasons to introduce a mass dependence to the effective interaction. First, as pointed out in Ref. ¹⁹, such a mass dependence is indispensable to reproduce all the nuclei from small to large mass numbers. Second, since it is well known that the effective interaction is strongly density dependent, it is reasonable to have a mass dependence to relate various cluster effects with mass. Third, the good agreement of many nuclear properties calculated using this parameter set with those from the parameter set NL3 also supports such a mass dependence.

5. Acknowledgments

L.S. Geng is grateful to the Monkasho fellowship for supporting his stay at Research Center for Nuclear Physics where this work is carried out. This work was partly supported by the Major State Basic Research Development Program Under Contract Number G2000077407 and the National Natural Science Foundation of China under Grant No. 10025522, 10221003 and 10047001.

References

1. T.H.R. Skyrme, *Phil. Mag.* **1**, 1043 (1956).
2. J. Decharge and D. Gogny, *Phys. Rev.* **C21**, 1568 (1980).
3. H. Flocard, P. Quentin and D. Vautherin, *Phys. Lett.* **B46**, 304 (1973).
4. J.D. Walecka, *Ann. Phys. (N.Y.)* **83**, 491 (1974).
5. B.D. Serot and J.D. Walecka, *Adv. Nucl. Phys.* **16**, 1 (1986).
6. P.G. Reinhard, *Rep. Prog. Phys.* **52**, 439 (1989).
7. I. Tanihata, *Prog. Part. Nucl. Phys.* **35**, 505 (1995).
8. D. Hirata, H. Toki, T. Watabe, I. Tanihata and B.V. Carlson, *Phys. Rev.* **C44**, 1467 (1991).
9. P. Ring, *Prog. Part. Nucl. Phys.* **37**, 193 (1996).
10. Y.K. Gambhir, P. Ring and A. Thimet, *Ann. Phys. (N.Y.)* **194**, 132 (1990).
11. N. Sandulescu, Nguyen Van Giai and R.J. Liotta, *Phys. Rev.* **C61**, 061301(R) (2000).
12. M. Grasso, N. Sandulescu, Nguyen Van Giai and R. J. Liotta, *Phys. Rev.* **C64**, 064321 (2001).
13. J. Meng and P. Ring, *Phys. Rev. Lett.* **77**, 3963 (1996).
14. J. Meng, *Nucl. Phys.* **A635**, 3 (1998).
15. H.L. Yadav, S. Sugimoto and H. Toki, *Mod. Phys. Lett.* **A17**, 2523 (2002).
16. N. Sandulescu, L.S. Geng, H. Toki and G.C. Hillhouse, *Phys. Rev.* **C68**, 054323 (2003).
17. H.L. Yadav, M. Kaushik and H. Toki, *nucl-th/0402013*.
18. L.S. Geng, H. Toki, S. Sugimoto and J. Meng, *Prog. Theor. Phys.* **110**, 921 (2003).
19. L.S. Geng, H. Toki, A. Ozawa and J. Meng, *Nucl. Phys.* **A730**, 80 (2004).
20. L.S. Geng, H. Toki and J. Meng, *Phys. Rev.* **C68**, 061303(R) (2003).

14 *L. S. Geng, H. Toki, and J. Meng*

21. J. Meng and P. Ring, Phys. Rev. Lett. **80**, 460 (1998).
22. J. Eberth, R.A. Meyer and K. Sistemich (ed.), *Nuclear Structure of the Zirconium Region* (Springer, Berlin, 1988).
23. J.L. Wood, K. Heyde, W. Nazarewicz, M. Huyse and P. Van Duppen, Phys. Rep. **215**, 101 (1992).
24. J. Skalski, S. Mizutori and W. Nazarewicz, Nucl. Phys. **A617**, 282 (1997).
25. P. Möller, J.R. Nix, W.D. Myers and W.J. Swiatecki, At. Data Nucl. Data Tables **59**, 185 (1995).
26. S. Goriely, F. Tondeur and J.M. Pearson, At. Data Nucl. Data Tables **77**, 311 (2001).
27. A.L. Goodman, Phys. Rev. **C60**, 014311 (1999).
28. S.G. Zhou, J. Meng and P. Ring, Phys. Rev. **C68**, 034323 (2003).
29. C. Samanta and S. Adhikari, *nucl-th/0402016*; Phys. Rev. **C65**, 037301 (2002).
30. J. Meng, K. Sugawara-Tanabe, S. Yamaji, P. Ring and A. Arima, Phys. Rev. **C58**, 628(R) (1998); J. Meng, K. Sugawara-Tanabe, S. Yamaji and A. Arima, Phys. Rev. **C59**, 154 (1999).
31. J. Meng and I. Tanihata, Nucl. Phys. **A650**, 176 (1999).
32. G.A. Lalazissis, D. Vretenar and P. Ring, Phys. Rev. **C57**, 2294 (1998).
33. Shouichi Sakakihara and Yasutoshi Tanaka, Nucl. Phys. **A691**, 649 (2001).
34. Y. Sugahara and H. Toki, Nucl. Phys. **A579**, 557 (1994); Y. Sugahara, Ph.D. thesis, Tokyo Metropolitan University, 1995.
35. G.A. Lalazissis, J. König and P. Ring, Phys. Rev. **C55**, 540 (1997).
36. A.M. Lane, *Nuclear Theory* (Benjamin, 1964).
37. P. Ring and P. Schuck, *The Nuclear Many-body Problem* (Springer, 1980).
38. H. Flocard et al., Nucl. Phys. **A203**, 433 (1973).
39. G. Audi and A.H. Wapstra, Nucl. Phys. **A595**, 409 (1995).
40. Wenhui Long, Jie Meng, Nguyen Van Giai and Shan-Gui Zhou, Phys. Rev. **C69**, 034319 (2004).
41. W. Nazarewicz, Nucl. Phys. **A654**, 195c (1999).
42. W. Satula, J. Dobaczewski and W. Nazarewicz, Phys. Rev. Lett. **81**, 3599 (1998).
43. H. Häkkinen et al., Phys. Rev. Lett. **78**, 1034 (1997).
44. S. Raman, C.W. Nestor, JR. and P. Tikkanen, At. Data Nucl. Data Tables **78**, 1 (2001).
45. K. Rutz, M. Bender, P.G. Reinhard, J.A. Maruhn and W. Greiner, Nucl. Phys. **A634**, 67 (1998).
46. H. De Vries, C.W. De Jager and C. De Vries, At. Data Nucl. Data Tables **36**, 495 (1987).

Table 1. The convergence study for ^{132}Sn with the parameter set TMA. Listed are the total binding energy, B , the binding energy per nucleon, B/A , the charge, neutron, proton, and matter root mean square radii, R_c , R_n , R_p and R_m , and the quadrupole deformation parameter for the neutron, proton and matter distributions, β_{2n} , β_{2p} and β_{2m} . $N = N_b = N_f$ is the number of shells used for the expansion of fermion fields and boson fields.

N	B	B/A	R_c	R_n	R_p	R_m	β_{2n}	β_{2p}	β_{2m}
20	1103.464	8.360	4.7209	4.9764	4.6526	4.8563	0.000	0.000	0.000
18	1103.544	8.360	4.7203	4.9763	4.6520	4.8560	0.000	0.000	0.000
16	1103.760	8.362	4.7197	4.9750	4.6514	4.8550	0.000	0.000	0.000
14	1103.735	8.362	4.7216	4.9749	4.6533	4.8556	0.000	0.000	0.000
12	1103.258	8.358	4.7211	4.9772	4.6528	4.8569	0.000	0.000	0.000
10	1101.932	8.348	4.7180	4.9669	4.6497	4.8492	0.000	0.000	0.000

Table 2. The same as Table I, but for ^{176}Sn .

N	B	B/A	R_c	R_n	R_p	R_m	β_{2n}	β_{2p}	β_{2m}
20	1174.685	6.674	5.0843	5.7995	5.0209	5.5894	0.000	0.000	0.000
18	1174.621	6.674	5.0841	5.7961	5.0207	5.5868	0.000	0.000	0.000
16	1174.314	6.672	5.0837	5.7886	5.0204	5.5811	0.000	0.000	0.000
14	1174.119	6.671	5.0853	5.7810	5.0220	5.5759	0.000	0.000	0.000
12	1171.623	6.657	5.0862	5.7533	5.0229	5.5556	0.000	0.000	0.000
10	1153.970	6.557	5.0745	5.6764	5.0110	5.4956	0.000	0.000	0.000

Table 3. The same as Table I, but for ^{130}Zr .

N	B	B/A	R_c	R_n	R_p	R_m	β_{2n}	β_{2p}	β_{2m}
20	936.601	7.205	4.6343	5.3251	4.5647	5.1032	-0.218	-0.171	-0.203
18	936.578	7.204	4.6346	5.3171	4.5651	5.0975	-0.215	-0.171	-0.202
16	936.380	7.203	4.6363	5.3036	4.5667	5.0883	-0.213	-0.172	-0.200
14	936.075	7.201	4.6390	5.2893	4.5695	5.0787	-0.208	-0.172	-0.197
12	934.880	7.191	4.6416	5.2637	4.5722	5.0610	-0.199	-0.171	-0.190
10	928.696	7.144	4.6462	5.2038	4.5768	5.0185	-0.181	-0.168	-0.177

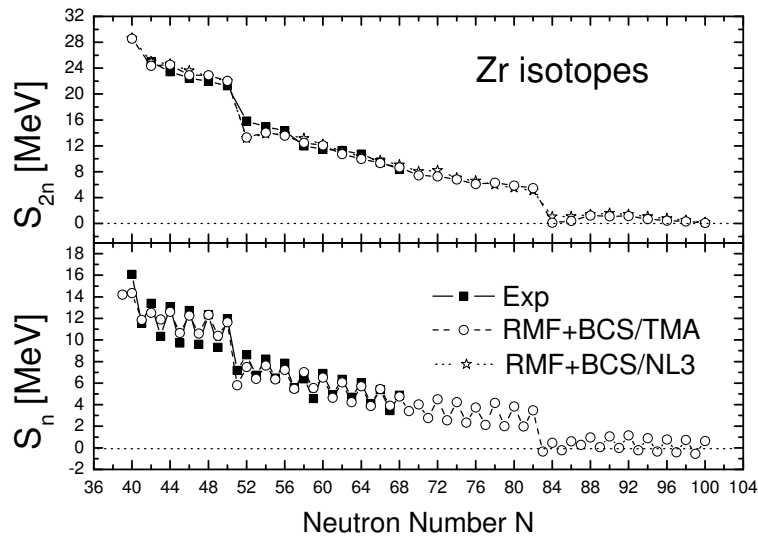


Fig. 1. The double and single neutron separation energies, S_{2n} and S_n , of Zr isotopes. The results obtained from the deformed RMF+BCS calculations with TMA set (open circle) are compared with available experimental data (solid square). In the upper panel, the results obtained from the deformed RMF+BCS calculations with NL3 set (open star) are also shown for comparison.

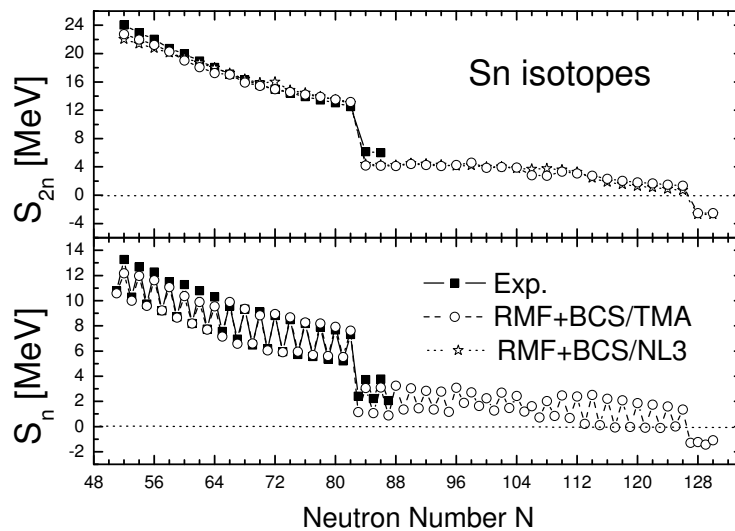


Fig. 2. The same as Fig. 1, but for Sn isotopes.

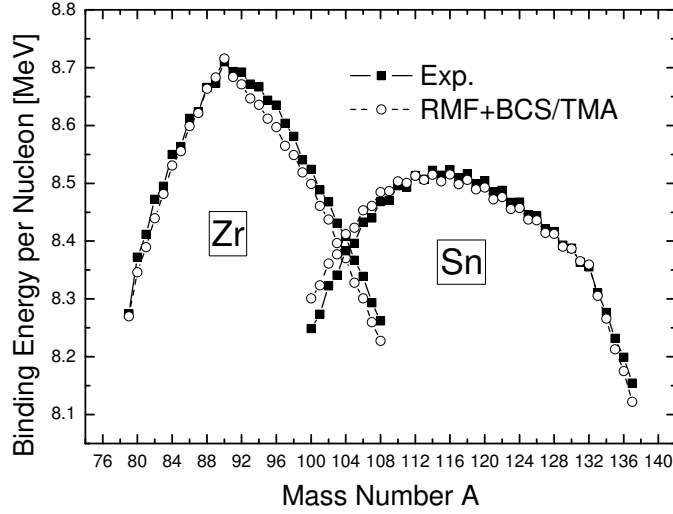


Fig. 3. The binding energies per nucleon of Zr and Sn isotopes. The results obtained from the deformed RMF+BCS calculations with TMA set (open circle) are compared with available experimental data (solid square).

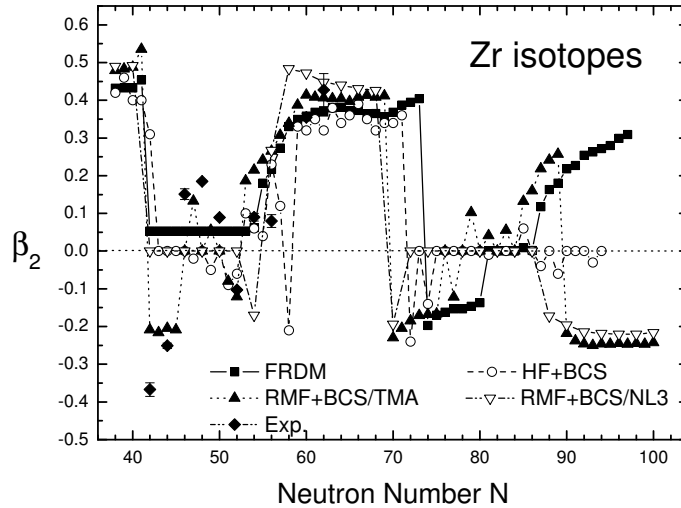


Fig. 4. The mass quadrupole deformation parameters, β_2 , of Zr isotopes. The results obtained from the deformed RMF+BCS calculations with TMA set (solid up-triangle) and NL3 set (empty down-triangle) are compared with those of finite range droplet model (FRDM) (solid square), those of Hartree Fock + BCS (HF+BCS) method (empty circle) and those extracted from the $B(E2)$ values (solid diamond with error bar). The results from the RMF+BCS/NL3 calculations are only shown for even-even nuclei.

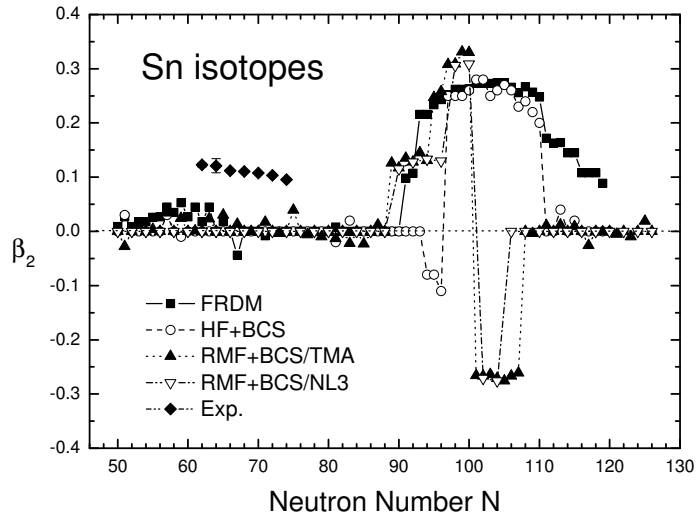


Fig. 5. The same as Fig. 4, but for Sn isotopes.

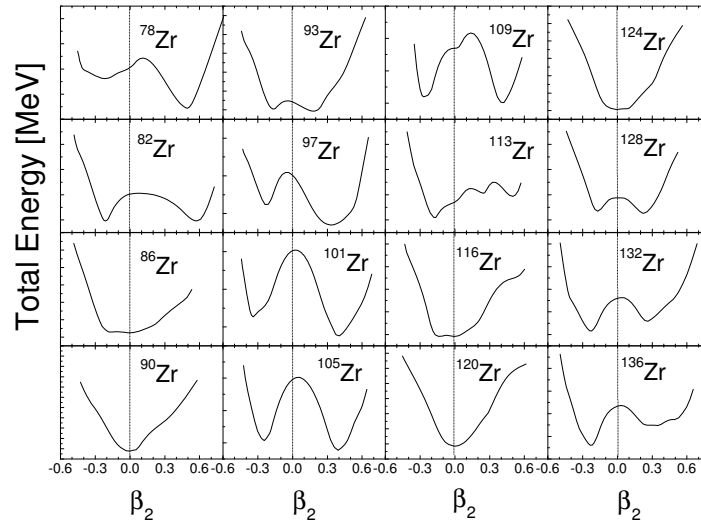


Fig. 6. The total energy curves of 16 Zr isotopes obtained from the deformed RMF+BCS calculations with TMA set as functions of mass quadrupole deformation parameters, β_2 .

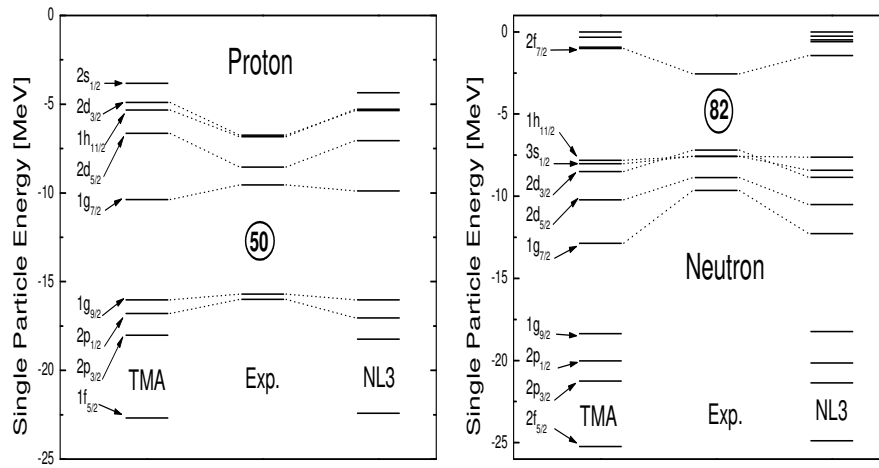


Fig. 7. The proton and neutron single-particle spectra of ^{132}Sn . The results obtained from the deformed RMF+BCS calculations with TMA and NL3 parameter sets are compared with available experimental data.

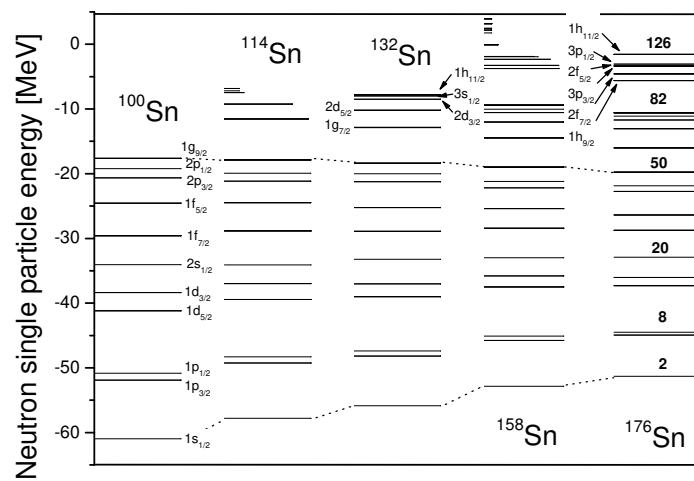


Fig. 8. The neutron single-particle spectra of ^{100}Sn , ^{114}Sn , ^{132}Sn , ^{158}Sn and ^{176}Sn obtained from the deformed RMF+BCS calculations with TMA set.

20 *L. S. Geng, H. Toki, and J. Meng*

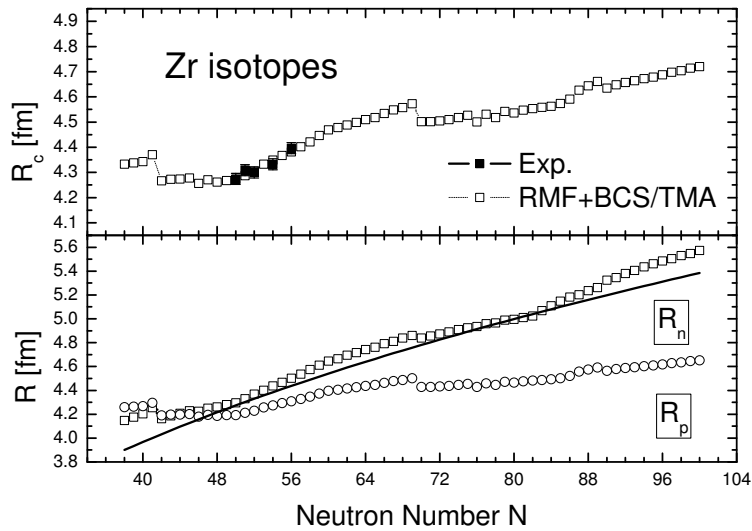


Fig. 9. The charge, proton and neutron radii obtained from the deformed RMF+BCS calculations with the TMA parameter set (open square and circle) compared with available experimental data (solid square). The solid line denotes a $N^{1/3}$ dependence.

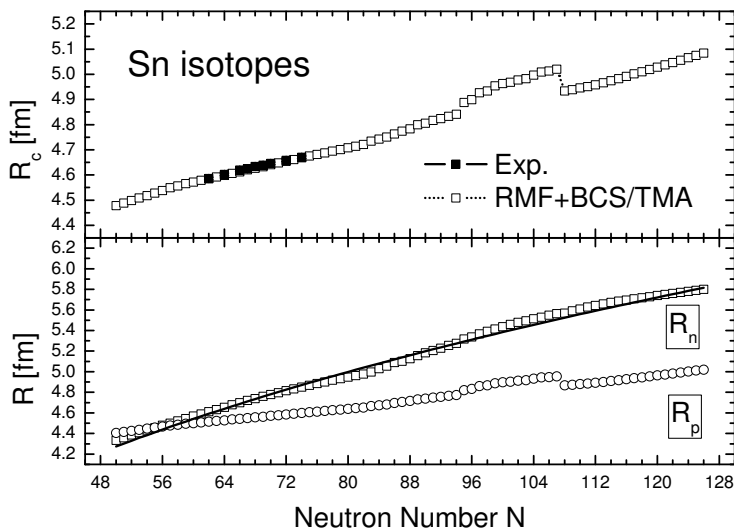


Fig. 10. The same as Fig. 9, but for Sn isotopes.